JOURNAL OF NEUROPHYSIOLOGY
Vol. 72, No. 2, August 1994. *Printed in U.S.A.*

Synaptic Integration in a Model of Cerebellar Granule Cells

FABRIZIO GABBIANI, JENS MIDTGAARD, AND THOMAS KNÖPFEL
Institut für Theoretische Physik, ETH-Hönggerberg, CH-8093 Zürich, Switzerland; and Institute of Neurophysiology, University of Copenhagen, DK-2200 Copenhagen N, Denmark

SUMMARY AND CONCLUSIONS

1. We have developed a compartmental model of a turtle cerebellar granule cell consisting of 13 compartments that represent the soma and 4 dendrites. We used this model to investigate the synaptic integration of mossy fiber inputs in granule cells.

2. The somatic compartment contained six active ionic conductances: a sodium conductance with fast activation and inactivation kinetics, g_{Na}; a high-voltage-activated calcium conductance, $g_{Ca(HVA)}$; a delayed potassium conductance, $g_{K(DR)}$; a transient potassium conductance, $g_{K(A)}$; a slowly relaxing mixed Na^+/K^+ conductance activating at hyperpolarized membrane potentials, g_H, and a calcium- and voltage-dependent potassium conductance, $g_{K(Ca)}$. The kinetics of these conductances was derived from electrophysiological studies in a variety of preparations, including turtle and rat granule cells.

3. In the soma, dynamics of intracellular free Ca^{2+} was modeled by incorporation of a Na^+/Ca^{2+} exchanger, radial diffusion, and binding sites for Ca^{2+}.

4. The model of the turtle granule cell exhibited depolarization-induced action potential firing with properties closely resembling those seen with intracellular recordings in turtle granule cells in vitro.

5. In the most distal compartments of the dendrites, mossy fiber activity induced synaptic currents mediated by α-amino-3-hydroxy-5-methyl-4-isoxazolepropionic acid (AMPA)- and *N*-methyl-D-aspartate (NMDA)-type of glutamate receptors. The strength of synaptic inputs chosen was such that the synaptic potential induced by synchronous activation of two mossy fiber synapses reached threshold for induction of a single action potential.

6. The slow time course of the NMDA synaptic current together with the slow relaxation kinetics of g_H significantly affected the temporal summation of excitatory synaptic potentials. A priming action potential evoked by mossy fiber stimulation increased the maximal time interval between two synaptic potentials capable to reach again threshold for a subsequent action potential. This time interval then decreased in parallel with the decay of the NMDA synaptic current, reached a minimum after 200 ms, and slowly recovered with reactivation of g_H.

7. Repetitive, steady activation of synaptic conductances by a single mossy fiber at different frequencies induced action potential firing with a sharp threshold at 12 Hz. Activity of a single or of several mossy fibers induced firing of the granule cell at a frequency close to that induced when the average synaptic current was directly injected into the cell. The mossy fiber activity-granule cell firing frequency curve was close to linear with a slope of about one-half for input frequencies ≤400 Hz.

8. The effects of Golgi cell inhibition on mossy fiber to granule cell transmission were studied by inserting constant Cl^- [γ-aminobuturic acid-A ($GABA_A$)]-conductances proximal to the mossy fiber synapses. With small values of the tonic inhibitory conductance, the temporal summation of repetitive synaptic potentials generated from two mossy fiber inputs became more dependent on their interspike interval, with maximal efficacy for coinciding inputs. Higher values of the tonic inhibitory conductance caused a shift of the output frequency versus mossy fiber frequency curve towards higher input frequency values. These two effects, taken together, suggest that Golgi cell feed forward and feed backward inhibition results in an increased sensitivity of parallel fiber output on the timing of mossy fiber inputs impinging on a single granule cell.

9. We conclude that granule cells are electrotonically very compact; the NMDA component of mossy fiber excitatory postsynaptic potentials can play an important role in synaptic integration by favoring temporal summation of excitatory inputs, and Golgi cell inhibition is a powerful regulator of the sensitivity of parallel fiber output on the timing of mossy fiber inputs. These aspects of synaptic integration are relevant to the early processing of mossy fiber input by the cerebellar cortex.

INTRODUCTION

The cerebellar granule cells are excitatory interneurons that relay mossy fiber inputs via parallel fibers to Purkinje cells and other neurons in the cerebellar cortex. On the average, each granule cell receives excitatory connections from only 4–5 mossy fibers, which synapse on granule cell dendrites in the cerebellar glomeruli. During voluntary limb or eye movements, for example, mossy fibers are capable of firing at frequencies well exceeding 100 Hz (Ariel and Fan 1993; Kase et al. 1980; van Kan et al. 1993). These high-frequency signals might encode different parameters of the ongoing movement, such as velocity or position signals. On the other hand, granule cell axons terminate as parallel fibers in the molecular layer of the cerebellar cortex, where they contact mainly Purkinje cell dendrites by means of presynaptic varicosities. Because each Purkinje cell receives >100,000 parallel fiber inputs (Napper and Harvey 1988a,b), it is unlikely that most of them are active at the high-frequency registered in mossy fibers. Hence, one would expect granule cells to perform some kind of reduction or filtering of mossy fiber input before distributing it to Purkinje cells. On theoretical grounds it also has been argued that a sparse coding of the parallel fiber input to the Purkinje cell would result in an optimal information storage capacity of the cerebellar cortex (Marr 1969).

However, because of their small membrane time constant compared with other cerebellar cells, their electrical compactness, and their expression of fast Na^+ channels, granule cells are expected to be rather excitable and capable of firing at high frequencies. Indeed, available experimental evidence revealed high-frequency firing of granule cells during intracellular injection of depolarizing current pulses in cerebellar slices (J. Midtgaard, see RESULTS, and E. D'Angelo, unpublished observations). Several possible mechanisms that could mediate an efficient reduction of parallel fiber activity relative to mean mossy fiber activity

are conceivable: these include nonlinear interaction of excitatory synaptic inputs impinging on the granule cell, timing effects between different mossy fiber signals, interaction of synaptic conductances with intrinsic membrane conductances, and Golgi cell inhibition. To investigate which of these effects is likely to play a significant role in the integration of mossy fiber input, we have constructed a compartmental model, compared its behaviour with intracellular recordings from turtle granule cells in vitro, and explored some properties of synaptic integration.

At present, intracellular recording of granule cells was done mainly on rats and turtles. Most voltage-clamp studies on active channels and mossy fiber transmission were performed in rat granule cell cultures and slices, whereas current-clamp data on intrinsic membrane properties are available in turtle granule cells. Hence our modeling necessarily had to borrow experimental results from these two species. Our choice to study synaptic integration in turtle granule cells rather than rats is motivated by the fact that experimental current-clamp data lie close to the problems we wish to study. In addition, other cerebellar cells have been studied in turtles (Midtgaard 1992), and this paper is part of an effort to model the cerebellar circuitry.

METHODS

Electrophysiology

Cerebellar tissue was isolated from turtles (*Trachemys scripta elegans*) as previously described in detail (Hounsgaard and Midtgaard 1988; Midtgaard 1992). Whole cell patch-clamp recordings from granule cells in vitro were obtained by closely following the method of Blanton et al. (1989). Recording electrodes contained (in mM): 117 K-gluconate, 3.3 $MgCl_2$, 2.3 Mg-gluconate, 0.36 $CaCl_2$, 0.5 ethylene glycol-bis(β-aminoethyl ether)-*N,N,N',N'*-tetraacetic acid, 5 Na_2ATP, 10 *N*-2-hydroxyethylpiperazine-*N'*-2-ethanesulfonic acid, 5 glucose, pH 7.6. Recordings were done at room temperature (22–24°C) in current clamp mode (DC-10 kH) using an Axoclamp-2A amplifier (Axon Instruments). Further experimental details will be presented elsewhere.

Morphology and electrotonic parameters of the model

The morphological structure of the model is shown in Fig. 1*B*. The cell consisted of a spherical soma and four cylindrical dendrites each of which terminates with a cylindrical dendritic bulb (Mugnaini et al. 1974). The dimensions were as follows: radius of the soma, 5 μm; radius of the dendrites, 0.62 μm; length of a dendrite, 88.1 μm; radius and length of the dendritic bulbs, 1.8 μm and 7.2 μm, respectively. The specific membrane capacity was 1 $\mu F/cm^2$ and the specific longitudinal (cytoplasmic) resistivity was 100 $\Omega \cdot cm$, in accordance with a previous passive model of rat granule cells (Silver et al. 1992). In the dendrites, the membrane resistance times unit area was 30,300 $\Omega \cdot cm^2$ (corresponding to a conductance of 33 $\mu S/cm^2$) and was set in series with a −65 mV battery. Each dendrite had a length of 0.09 in electrotonic units and was separated in two compartments representing <0.05λ of electrotonic length. The electrotonic contribution of the axon was neglected. In the soma, resting membrane conductance resulted from resting activity of potassium conductances (76 $\mu S/cm^2$), a mixed Na^+/K^+ inward rectifier (13 $\mu S/cm^2$), and from sodium and calcium leak conductances of 7.6 $\mu S/cm^2$ and 4 $\mu S/cm^2$, respectively. The calcium leak current ensured a resting calcium concentration of 75.5 nM.

Small hyperpolarizing current pulses (10 pA) delivered at resting membrane potential revealed an input resistance of 1.1 $G\Omega$ and a system time constant of 16 ms.

Active membrane conductances

As the location of membrane channels was not yet explored experimentally, active conductances only were included in the somatic compartment. This simplification had no influence on the aspects explored here, because the length of granule cell dendrites is electrotonically very short (see also RESULTS). The general formalism to describe the kinetics of active channels derives from the Hodgkin-Huxley equations. In general, the activity of a conductance g_x is a function of two state variables, x_a and x_i, which reflect activation and inactivation mechanisms of the channel and whose values lie between 0 and 1,

$$g_x = \bar{g}_x \cdot x_a^{n_x} \cdot x_i.$$

In this equation, the constant $\bar{g}_x$ denotes the maximal value of the conductance g_x and the integer n_x represents the number of activation gates of the channel [$n_x > 1$ introduces a delay in channel activation (Hodgkin and Huxley 1952)]. The kinetics of state variables is described by first order differential equations

$$\frac{dx_j}{dt} = \alpha_{x_j} \cdot (1 - x_j) - \beta_{x_j} \cdot x_j, \quad j = a, i,$$

where the rate functions for activation and inactivation α_{x_j} and β_{x_j} depend on voltage. The steady-state value of x_j, $x_{j\infty}$, and its relaxation time constant, τ_{x_j}, are given by

$$x_{j\infty} = \frac{\alpha_{x_j}}{\alpha_{x_j} + \beta_{x_j}},$$

$$\tau_{x_j} = \frac{1}{\alpha_{x_j} + \beta_{x_j}}, \quad j = a, i.$$

The kinetic model used to describe $I_{K(Ca)}$ depends on calcium concentration as well as on voltage and will be described separately below.

To describe the voltage dependence of the various rate functions, expressions consistent with experimental data from voltage-clamp experiments were searched for. For most channels, a scheme based on a set of simple expressions described by Borg-Graham (1987, 1991) was found to fit data with sufficient accuracy. The rate functions and maximal conductances (except that of $I_{K(Ca)}$), as well as the reversal potentials of these currents are summarized in Table 1. Some justifications and comments follow.

An inactivating sodium conductance, g_{Na}, was modeled assuming conventional m^3h kinetics with activation and inactivation state variables m and h. Rate functions were obtained by fitting terms of the Borg-Graham type to voltage-clamped currents of this channel observed in rat granule cells (Cull-Candy et al. 1989). The Borg-Graham rate functions require lower limits for relaxation time constants, which were chosen to be 0.05 and 0.225 ms for activation and inactivation rate functions, respectively. The maximal conductance provided by this channel, $\bar{g}_{Na}$, was 70 mS/cm^2, a value large enough to obtain overshooting action potentials. The reversal potential for Na^+, E_{Na}, was 55 mV.

A delayed potassium conductance, $g_{K(DR)}$, was modeled by fitting n^4i kinetics to voltage-clamped currents described in rat granule cells (Cull-Candy et al. 1989). The inactivation of $g_{K(DR)}$ was chosen to be similar to the one described in hippocampal CA1 pyramidal cells (Sah et al. 1988). Inactivation of $g_{K(DR)}$ was necessary to replicate voltage-clamp experiments of Cull-Candy et al. (1989), but was of minor significance during subsequent simulations because of its slow kinetics and because repolarization of action potentials resulted mainly from the action of $g_{K(Ca)}$ (see

TABLE 1.

Process, state variables	$\bar{g}_x$, mS/cm^2	n_x	E_x, mV	Forward Rate Constants α_{x_a} or α_{x_i}, ms^{-1}	Backward Rate Constants β_{x_a} or β_{x_i}, ms^{-1}	τ_{min}, ms
g_{Na}						
Activation m	70	3	55	$1.5e^{[0.081(V+39)]}$	$1.5e^{[-0.066(V+39)]}$	0.05
Inactivation h				$0.12e^{[-0.089(V+50)]}$	$0.12e^{[0.089(V+50)]}$	0.225
$g_{K(DR)}$						
Activation n	19	4	−90	$0.17e^{[0.073(V+38)]}$	$0.17e^{[-0.018(V+38)]}$	0
Inactivation i				$0.0007 + 6.5e^{[-0.08(V+46)]}$	$110 \cdot 10^{-5}/\{1 + e^{[-0.0807(V-44)]}\}$	0
$g_{K(A)}$						
Activation a	3.67	3	−90	$0.35e^{[0.039(V+70)]}$	$0.35e^{[-0.091(V+70)]}$	0.16
Inactivation b				$0.175e^{[-0.02(V+80)]}$	$0.175e^{[0.18(V+80)]}$	12
$g_{Ca(HVA)}$						
Activation s	2.91	2	80	$1.6/\{1 + e^{[-0.072(V-5)]}\}$	$-0.02(V - 8.9)/[1 - e^{-0.2(V-8.9)}]$	0
Inactivation t				$0.005e^{[-0.05(V+60)]}$	$0.005 - 0.005e^{[-0.05(V+60)]}$	0
g_H						
Activation d	0.09	1	−42	$0.0008e^{[-0.0909(V+75)]}$	$0.0008e^{[0.0909(V+75)]}$	0

$g_{K(DR)}$ inactivation, i, forward rate constant is equal to 0.00076 for $V > -46$ mV. Forward rate constant for $g_{Ca(HVA)}$ inactivation, t, is equal to 0.005 for $V < -60$ mV whereas its backward rate constant is equal to 0 for $V < -60$ mV.

below). The reversal potential for the current generated by this channel, $E_{K(DR)}$, was −90 mV.

A fast, transient potassium channel, $g_{K(A)}$, was modeled by fitting a^3b kinetics to voltage-clamped currents observed in rat granule cells (Cull-Candy et al. 1989). The maximal value of the conductance, $\bar{g}_{K(A)}$ was chosen such that this A-like current produced the typical deflection in voltage traces observed in the rising phase of action potentials during current-clamp experiments (see RESULTS).

For the high-voltage-activated (HVA) calcium conductance that was described in granule cells (De Waard et al. 1991; Marchetti et al. 1991; Slesinger and Lansman 1991), we used the s^2t kinetic model described by Traub et al. (1991) in their simulation of hippocampal CA3 pyramidal neurons. The channel carried little current and consequently its contribution to action potential depolarization was small. However, calcium influx associated with opening of $g_{Ca(HVA)}$ played an important role in the activation of $I_{K(Ca)}$. The maximal conductance of the channel, $\bar{g}_{Ca(HVA)}$, was chosen such that the rise in cytosolic calcium during an action potential sufficiently activated $I_{K(Ca)}$. $E_{Ca(HVA)}$ was set to 80 mV to account for Goldman-Hodgkin-Katz rectification (Hille 1992). A calcium channel with anomalous gating recently described in rat granule cells (Forti and Pietrobon 1993) was neglected.

An inward rectification is revealed in turtle granule cells by a sag in membrane potential during hyperpolarizing current pulses and by a rebound excitation following the pulses (Midtgaard, unpublished observations; see also RESULTS and Fig. 1*C*). It was modeled by introducing a slowly relaxing, mixed Na^+/K^+ conductance, g_H, and using equations developed for thalamic neurons (Huguenard and McCormick 1992; McCormick and Pape 1990). We assumed that the current carried by this conductance reversed at −42 mV and the time constant and maximal conductance were scaled to replicate the voltage deflections induced by hyperpolarizing current steps in turtle granule cells (see RESULTS).

Finally, the calcium-dependent potassium channel with large single-channel conductance observed in granule cells (Fagni et al. 1991), $g_{K(Ca)}$, was reported to exhibit kinetic properties similar to a channel studied by Moczydlowski and Latorre (1983) in artificial planar bilayers. The model proposed by these authors consists of three kinetic steps between two open and two closed states with two calcium-dependent steps between the open and closed states, respectively. We assumed the two calcium-dependent reactions to be at equilibrium, thus obtaining a simplified two-state model whose kinetic properties are summarized in the following diagram (Colquhoun and Hawkes 1981; Hille 1992)

$$C \underset{\tilde{\beta}}{\overset{\tilde{\alpha}}{\rightleftharpoons}} O$$

where,

$$\tilde{\alpha} = \frac{\beta}{1 + \frac{K_{1D}e^{-fV}}{[Ca^{2+}]_i}}, \quad \tilde{\beta} = \frac{\alpha}{1 + \frac{[Ca^{2+}]_i}{K_{4D}e^{-gV}}}.$$

The values of the kinetic parameters describing $g_{K(Ca)}$ were

$$\alpha = 1.5 \text{ ms}^{-1}, \quad f = 0.085 \text{ mV}^{-1}, \quad K_{1D} = 1.5 \ \mu\text{M},$$

$$\beta = 2.5 \text{ ms}^{-1}, \quad g = 0.077 \text{ mV}^{-1}, \quad K_{4D} = 150 \text{ nM}.$$

The dissociation constants K_{1D} and K_{4D} for the two calcium binding reactions (at 0 mV) were modified with respect to the ones put forth by Moczydlowski and Latorre to obtain a maximal calcium dependence of the channel at concentrations between 50 nM and 5 μM, as observed by Fagni et al. (1991).

The maximal conductance of the channel was set to 80 mS/cm^2 and $E_{K(Ca)}$ was −90 mV. We estimated the relative contribution of $g_{K(Ca)}$ and $g_{K(DR)}$ to the repolarization of action potentials from available voltage-clamp data of both channels (Cull-Candy et al. 1989; Fagni et al. 1991). With a ratio of $g_{K(Ca)}/g_{K(DR)} = 4.1$ as used in our model, spike repolarization was essentially due to the action of $g_{K(Ca)}$.

Calcium dynamics

Dynamics of intracellular calcium concentration was taken into account only in the soma, because all active conductances were located there. Calcium influx through *N*-methyl-D-aspartate (NMDA) channels was neglected. Radial diffusion of calcium in the soma was modeled by 12 shell-like concentric compartments (Yamada et al. 1989). The outermost six shells had a thickness of 0.1 μm followed by three shells of 0.5 μm thickness and three shells of 1 μm thickness. We used a value of 6×10^{-6} cm^2/s for the calcium diffusion constant D in aqueous solutions (Hodgkin and Keynes 1957; Robinson and Stokes 1955). Diffusion, however, was slowed due to the presence of calcium buffers. Each shell contained 25 μM of a kinetically fast buffer, exhibiting a single calcium binding site, with forward and backward rate constants of 30 mM$^{-1} \times$ ms^{-1} and 0.03 ms^{-1}, respectively (Sala and Hernandez-Cruz 1990).

Calcium extrusion was performed by a Na^+/Ca^{2+} exchanger with 3:1 stoichiometry located in the outermost shell of the cell body. The equation used for the exchanger was taken from studies

of cardiac cells (Kimura et al. 1987; Mullins 1977). The calcium current flowing through the exchanger (in $\mu A/cm^2$) was given by

$$i_{Ca} = -2k([Ca^{2+}]_o[Na^+]_i^3 e^{E_1 V} - [Ca^{2+}]_i[Na^+]_o^3 e^{-E_2 V}),$$

with $E_1 = 0.013\ mV^{-1}$ and $E_2 = 0.026\ mV^{-1}$, $[Ca^{2+}]_o = 2$ mM, $[Na^+]_o = 152$ mM and $[Na^+]_i = 9$ mM. The capacity k of the exchanger ($k = 4.677 \cdot 10^{-4} \frac{\mu A}{mM^4 cm^2}$), calcium leak conductance and buffer properties are a set of parameters that was adjusted to obtain a resting Ca^{2+} concentration of 75.5 nM, calcium transients decayed with a time constant of 144 ms, and 98% of calcium influx was trapped by the calcium binding buffer (Neher and Augustine 1992) at resting calcium concentration.

Excitatory synaptic conductances

Synaptic currents induced by mossy-fiber stimulation in rat granule cells are mediated by α-amino-3-hydroxy-5-methyl-4-isoxazolepropionoc acid (AMPA) as well as by NMDA receptors (D'Angelo et al. 1990, 1993; Silver et al. 1992). The AMPA receptor-mediated synaptic currents were modeled by a dual exponential function using parameters measured by Silver et al. (1992),

$$g_{AMPA}(t) = \bar{g}_{AMPA} \cdot 1.273 \cdot (e^{-t/\tau_{decay}} - e^{-t/\tau_{rise}}),$$

with $\tau_{rise} = 0.09$ ms and $\tau_{decay} = 1.5$ ms. The synaptic conductance peaks 270 μs after activation of the synapse. The maximal synaptic conductance ($\bar{g}_{AMPA} = 720$ pS) was four times larger than the peak conductance of AMPA miniature synaptic currents (Silver et al. 1992) in rat granule cells to account for the four times larger membrane area of turtle granule cells as compared with rat granule cells.

The NMDA receptor-mediated synaptic currents were modeled by a function, $g_{NMDA}(t)$, consisting of three terms describing the maximal conductance, $\bar{g}_{NMDA}$, the time course of the current following activation of the synapse and the voltage-dependence of the magnesium block, $g_\infty(V,[Mg^{2+}]_o)$,

$$g_{NMDA}(t) = \bar{g}_{NMDA} \cdot 1.358 \cdot (e^{-t/\tau_{decay}} - e^{-t/\tau_{rise}}) \cdot g_\infty(V,[Mg^{2+}]_o),$$

with $\tau_{rise} = 3$ ms and $\tau_{decay} = 40$ ms. The rise and decay time constants were in the range of values described by D'Angelo et al. (1992) and Silver et al. (1992) for NMDA miniature currents. For the voltage-dependent magnesium block, we used the gating function described by Jahr and Stevens (1990a)

$$g_\infty(V,[Mg^{2+}]_o) = \frac{1}{(1 + e^{-\alpha V}[Mg^{2+}]_o/\beta)},$$

with $\alpha = 0.062\ mV^{-1}$ and $\beta = 3.57$ mM. The external magnesium concentration, $[Mg^{2+}]_o$, was set to 1.2 mM. Notice that we assume the NMDA conductance to be in equilibrium with voltage and $[Mg^{2+}]_o$ so that the kinetics of the voltage-dependence of the channel (Jahr and Stevens 1990b) is not included. The NMDA synaptic current peaks 8.4 ms after activation of the synaptic mechanism. The value $\bar{g}_{NMDA} = 1.2$ nS was obtained from the mean peak NMDA miniature synaptic conductances reported by Silver et al. (1992) in rat granule cells, but was multiplied by four to account for the membrane area of turtle granule cells (see above).

Recently, the decay of whole-cell NMDA currents in rat granule cells has been reported to contain a second, slowly decaying component seen at depolarized membrane potentials (D'Angelo et al. 1993, 1994). This component was not included in the present model.

Because the mossy-fiber granule cell transmission consists of dual AMPA and NMDA components (D'Angelo et al. 1990; Silver et al. 1992), in most experiments both conductances were activated simultaneously. Excitatory synapses were placed at a voltage node located at the distal end of the granule cell dendritic bulbs (for details of implementation see Hines, 1993, Fig. 1). The reversal potential of the excitatory synaptic conductances was 0 mV.

Tonic Golgi cell inhibition

The effects of a tonic Golgi cell inhibition on mossy-fiber granule cell transmission were studied by including a passive Cl^- [γ-aminobutyric acid ($GABA_A$)]-conductance in the dendritic bulb compartment (Rall 1964). Thus Golgi cell inhibition always was located more proximal to the soma than mossy fiber excitation, in accordance with anatomic observations (Mugnaini et al. 1974). For simplicity, the reversal potential of Cl^- was set to the resting membrane potential, $E_{Cl^-} = -65$ mV. The value of $\bar{g}_{GABA_A}$ was varied in the range of 0 to 1.6 nS.

Numerical calculation of membrane voltage and calcium concentration time course

The dynamics of membrane voltage and calcium concentration in each cell compartment are determined by the discretized cable equation and diffusion equation, which were integrated numerically by means of a second-order implicit integration algorithm (Cooley and Dodge 1966; Mascagni 1989). The model was developed initially using a fast and accurate single cell simulator (Quadroni 1993). Simulations of 100 ms in current clamp took <1 min on a Sparc 2 Sun Station. At a later stage, the model was ported to the NEURON simulator (Hines 1989, 1993). Simulation of activity during synaptic stimulation was much more expensive in computer time. Thus NEURON was compiled with a special library (Condor) allowing to efficiently distribute simulations on 30 machines (Sun Sparc 1, 2, and 10) in batch mode. The electrical current flowing through the electrogenic Na^+/Ca^{2+} exchanger was negligible and was not taken into account for the calculation of membrane voltage. Care was taken to choose small enough time steps (usually 25 μs) to ensure numerical stability and the simulated cell was allowed to relax to its steady-state during 100 ms–1 s before initiating experimental protocols.

RESULTS

Intrinsic properties of the granule cell model

The model's responses to intrasomatic injection of depolarizing and hyperpolarizing current pulses are illustrated in Fig. 1*A*. The model cell does not show spontaneous activity. Injection of small depolarizing currents induces regular action potential firing with very little frequency accommodation. The action potentials have an amplitude of 67 mV (measured from rest), a half-width of 0.85 ms, and are followed by a pronounced spike after hyperpolarization (AHP), which has an amplitude of 4.2 mV when measured from resting (steady-state) potential (−65 mV). Repolarization from the AHP occurs in two phases: an initially fast return toward resting potential followed by a decrease in the rising rate of membrane potential. The latter effect results from the activity of $g_{K(A)}$ (Connor and Stevens 1971). The expression of g_H results in a time- and voltage-dependent inward rectification and a graded rebound excitation during and after hyperpolarizing current pulses, respectively.

Our model reproduces in these respects the main firing properties of turtle granule cells as seen with intracellular recordings in vitro (Fig. 1*C*), that is, the lack of a pronounced frequency accommodation, the spike amplitude and AHP, the dual component interspike trajectory of membrane potential under small depolarizing currents,

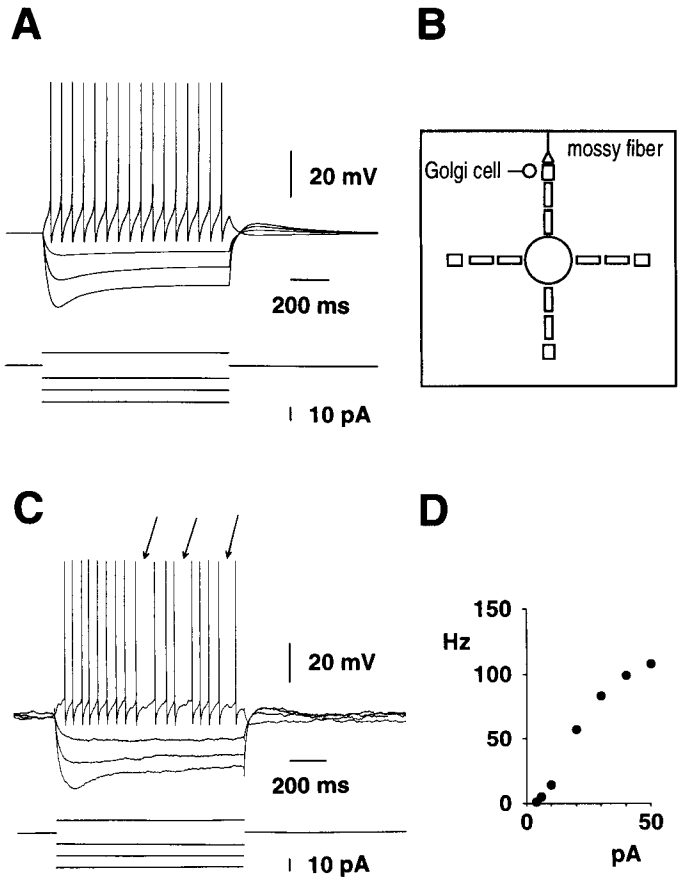

FIG. 1. Comparison of simulated and in vitro firing properties of turtle granule cells. *A*: response of the simulated granule cell to injection of a depolarizing current pulse and to hyperpolarizing current pulses (10, −10, −20, and −30 pA). *B*: morphological structure of the granule cell model and placement of excitatory and inhibitory synapses (not drawn to scale). *C*: whole cell recording from a turtle granule cell in current-clamp mode. Responses to depolarizing and hyperpolarizing current pulses (10, −10, −20, and −30 pA). Resting membrane potential was ~70 mV, no bias current. *D*: relationship between injected current and firing frequency obtained in another turtle granule cell.

and the initial sag in the membrane potential during hyperpolarizing pulses, which is followed by a hump depolarization at the end of the pulses. Note that in the experimental trace of Fig. 1*C* spontaneous inhibitory postsynaptic potentials (IPSPs) can prevent action potential generation as indicated by the occasional occurrence of double-sized interspike intervals (Fig. 1*C*, arrows). The injected current versus firing frequency curve obtained in a different granule cell is shown in Fig. 1*D*. The simulated current frequency curve of the model is in the range of observed experimental values (see Fig. 4*B* and below).

Figure 2 shows the membrane voltage and submembraneous calcium concentration during an action potential as well as the time course of the currents flowing through the membrane. The current flowing through HVA calcium channels contributes little to spike depolarization (Fig. 2*A3*), but causes a raise in intracellular calcium concentration (Fig. 2*A1*), which activates the calcium-dependent potassium current $I_{K(Ca)}$. Spike repolarization is mainly due to the action of $I_{K(Ca)}$ (Fig. 2*A2*), which activates immediately after the fast sodium current, and to a much smaller extend, to the delayed rectifier. After the spike AHP, the A channel activates upon membrane repolarization (see Fig. 2*A3*). Figure 2*B3* shows the activation variable of the H channel: the channel closes during the action potential and slowly reopens afterwards, whereas the H current relaxes to its resting value (Fig. 2*B2*).

Induction of action potential firing by mossy fiber inputs

Figure 3*A* shows the effect of activating AMPA, NMDA, or mixed AMPA/NMDA type of synaptic conductances on somatic membrane potential and the corresponding synaptic currents flowing in the dendritic bulb. The nearly instantaneous rise of the AMPA conductance causes a fast increase in membrane potential that peaks at −61.9 mV after 4.1 ms. Concurrent activation of the NMDA conductance only slightly increases the peak value of membrane voltage to −60.9 mV, however. The slow conductance decay,

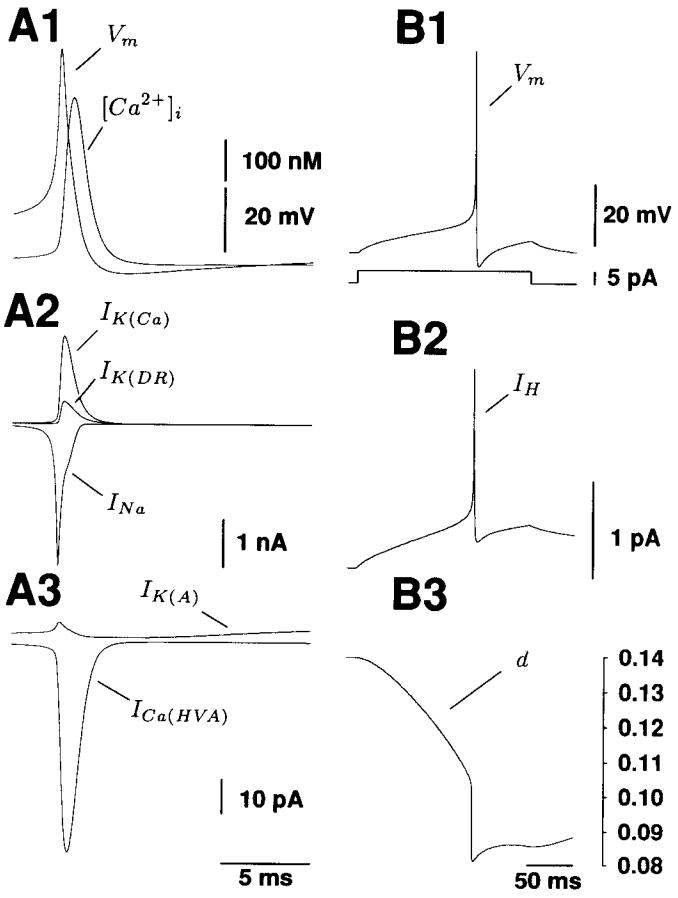

FIG. 2. Time course of somatic membrane voltage, submembraneous calcium concentration, and ionic currents flowing across the membrane during an action potential. The action potential was elicited by a 5 pA current pulse of 190 ms duration (see *B1*). *A1*: membrane voltage (V_m) and submembraneous calcium concentration ($[Ca^{2+}]_i$, peak value 900 nM). *A2*: fast sodium current (I_{Na}, peak value 3.0 nA), delayed rectifier current ($I_{K(DR)}$, peak value 0.47 nA), and current mediated by calcium-activated potassium channels ($I_{K(Ca)}$, peak value 1.8 nA). *A3*: high-voltage-activated (HVA) calcium current ($I_{Ca(HVA)}$, peak value 62 pA) and A current ($I_{K(A)}$, end value 3.5 pA). *B1*: action potential induced by a depolarizing current (5 pA) plotted on a faster time scale. *B2*: H current (I_H resting value 0.9 pA). *B3*: time course of the activation variable d of I_H. Note the different time scales between *A* and *B*, as well as the different current scales in *A2*, *A3*, and *B2*.

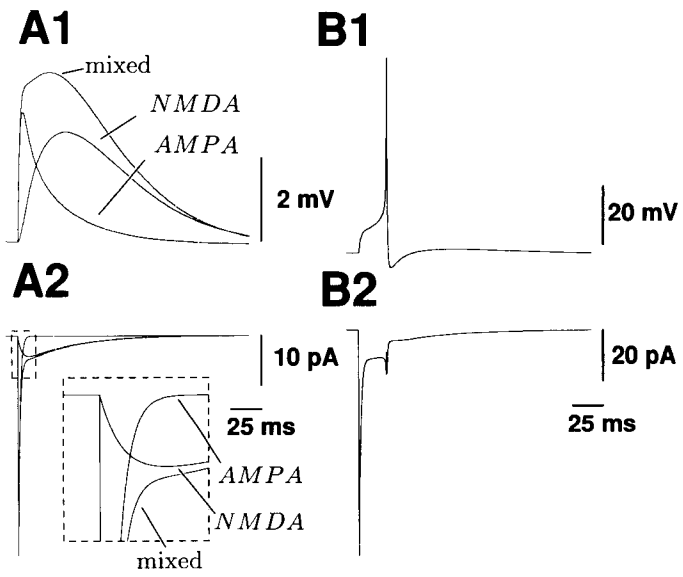

FIG. 3. Synaptic currents and voltage during activation of mossy fiber synapses. *A1*: somatic membrane voltage during activation of α-amino-3-hydroxy-5-methyl-4-isoxazolepropionic acid (AMPA), *N*-methyl-D-aspartate (NMDA), and mixed AMPA/NMDA synapses. *A2*: currents flowing through the synaptically activated channels (peak current values are AMPA: 45 pA, NMDA: 4.2 pA, and mixed AMPA/NMDA: 45 pA). The inset shows on an expanded scale part of the rising and falling phase of the currents (width and height of dotted box is 20 ms and 9.5 pA). *B1*: somatic membrane voltage after simultaneous activation of 2 mixed AMPA/NMDA synapses. *B2*: corresponding synaptic current (peak value: 90 pA).

which is characteristic for this channel, induces a depolarization lasting >100 ms. In Fig. 3*B*, two synapses activated simultaneously cause the cell to fire an action potential. Activation of the synapses results in an initial fast depolarization of the cell because of the AMPA component of the synaptic current. The subsequent slower depolarization, which finally reaches threshold for action potential generation, results from the persistent action of the NMDA and H current as well as the slow inactivation of $I_{K(A)}$.

Does continuous, repetitive mossy fiber activity drive the granule cell to regular steady-state firing of action potentials? Plotting the granule cell firing frequency against the frequency of mossy fiber activity (Fig. 4*A*, ●) yields a curve (*f-F* curve) that is approximately linear, indicating linear summation of mossy fiber inputs, and has a slope of 1/2, reflecting the fact that two synaptic inputs are required to fire the cell.

Excitatory postsynaptic potentials (EPSPs) impinging on different granule cell dendrites might interact differently than EPSPs arising at a single dendritic bulb. We investigated this possibility by comparing the *f-F* curve with the firing frequency curve obtained by stimulating for a given frequency each of the four mossy fiber inputs of the cell in turn at one-quarter of the frequency. That is, we distributed a given frequency input evenly between the four dendrites. The result of this simulation is also shown on Fig. 4*A* (▽). The two curves of Fig. 4*A* are remarkably similar up to a stimulation frequency of 150 Hz. At higher frequencies, a single mossy fiber drives the granule cell more effectively. Calculation of *f-F* curves with activation of either AMPA or NMDA conductances alone revealed that this is due to the nonlinearity of the NMDA current (not illustrated). The increased efficacy of NMDA channels when stimulated in one bulb at high frequency is due to a relief of the voltage-dependent Mg^{2+} block, as can be seen by plotting the mean voltage in each bulb (not illustrated). A similar effect due to clustering of NMDA synapses has been observed in simulations of cortical pyramidal cells (Mel 1992, 1993). We conclude from this that spatial segregation of mossy fiber inputs has a negligible effect on their integration by the simulated granule cell for a wide range of frequencies.

Small changes in synaptic conductances are capable to alter significantly the high input resistance of the granule cell model. Hence, we also compared the capabilities to drive the granule cell of current injected directly into the soma with current generated by activated synaptic conductances. For that, we plotted in Fig. 4*B* the granule cell firing frequency against the amplitude of directly injected constant current (*f-I* curve, ●). We further plotted the mean synaptic current induced by mossy fiber stimulation at varying frequencies versus output frequency (▽). Interestingly,

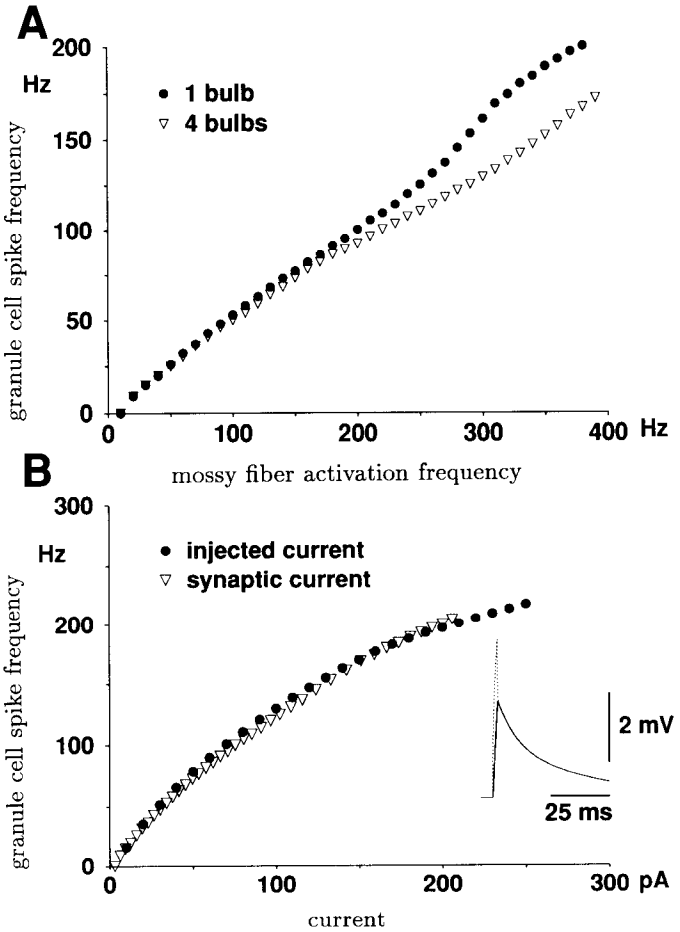

FIG. 4. Current vs. frequency and frequency vs. frequency plots. *A*: comparison of the firing frequency vs. mossy fiber stimulation frequency evenly distributed in 4 bulbs (▽) or in a single bulb (●). *B*: comparison of the firing frequency vs. intrasomatic injected current (●) and of the firing frequency vs. synaptic current averaged over several hundreds of milliseconds during mossy fiber stimulation at constant frequencies (▽). *Inset*: voltage response at different locations in the cell to a depolarizing current pulse (30 pA, 2 ms) injected in 1 dendritic bulb. The dashed line gives the voltage time-course at the site of current injection, and the 2 superposed filled lines are voltage in the soma and another dendritic bulb (baseline voltage: −65 mV).

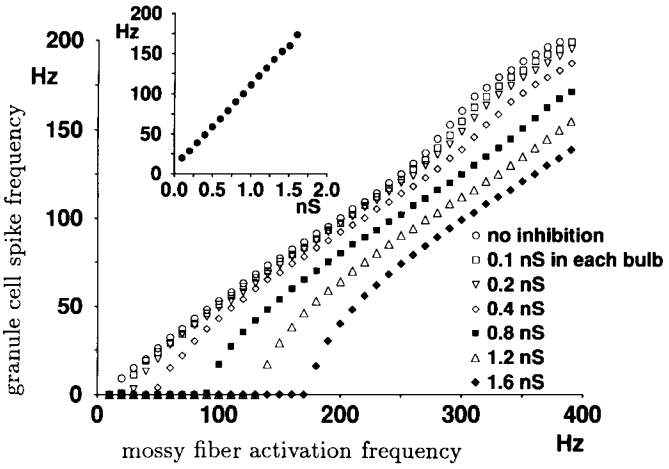

FIG. 5. Firing frequency of the granule cell vs. mossy fiber stimulation frequency for different values of tonic inhibition. *Inset* shows the minimal mossy fiber stimulation frequency able to induce action potential firing as a function of tonic inhibition.

this latter curve closely matches the relationship between injected current and firing frequency, showing that, in our model, current generated by synaptic conductances has a similar effect on the granule cell as a somatic current injection over a wide range of input frequencies. We further tested the compactness of the cell by injecting currents in the soma or in a dendritic bulb of the granule cell and comparing transients and steady-state attenuation of voltage at different locations in the cell. A short-lasting (2 ms) current injection into a dendritic bulb resulted in voltage transients in this bulb, the soma, and another bulb that were almost identical except for a very high-frequency component only seen at the site of current injection (Fig. 4*B, inset*). Steady-state attenuation factors, assessed with injection of small hyperpolarizing (1–2 pA) current pulses, between a bulb and the soma and between two bulbs were ≥ 0.99 and ≥ 0.94, respectively.

Role of inhibition on input-output firing relationship of granule cells

To investigate the role of Golgi cell inhibition on input-output relationship as revealed by *f-F* curves, a ohmic, $GABA_A$-like conductance was inserted in each dendritic bulb. This tonic conductance can be interpreted as asynchronous inhibitory background activity (Bernander et al. 1991) and, as the reversal potential of $GABA_A$ currents was set to membrane resting potential, it implements a "silent" inhibition (Koch et al. 1982; Kriegstein and Connors 1986). Indeed, it has been shown that Golgi cells are often spontaneously active both in vivo and in vitro (Eccles et al. 1967; Edgley and Lidierth 1987; van Kan et al. 1993).

Figure 5 shows the mean firing rate of the simulated granule cell versus mossy fiber stimulation frequency at different values of the tonic inhibitory conductance. In the absence of tonic inhibition, the minimal frequency needed to initiate an action potential lies between 10 and 20 Hz. Tonic inhibition induces two distinct effects: first, the *f-F* curve is shifted horizontally toward higher values of the mossy fiber input frequency. Thus inhibition shifts the threshold for action potential generation toward higher frequencies (Fig. 5, *inset*). Interestingly, inhibition had almost no effect on the slope of the *f-F* curve, as expected from the compactness of the cell (Vu and Krasne 1992). This effect of inhibition is independent of whether mossy fiber inputs are distributed over one or several dendritic bulbs and of the position of the inhibitory conductance on the granule cell dendrite. The second effect of tonic inhibition concerns the decoding of temporal patterns of mossy fiber inputs and will be described in the following.

Decoding of temporal input patterns

GAIN VERSUS PHASE RELATIONSHIP FOR TWO MOSSY FIBER INPUTS AS A FUNCTION OF INHIBITION. From a theoretical point of view, the kinetic properties of AMPA and NMDA subtypes of glutamate-activated receptors imply very different roles for these channels in the integrative properties of a neuron (Softky and Koch 1993). On the one hand, fast activation and inactivation of AMPA currents requires that inputs almost coincide to be temporally summated and favors synchronization of synaptic events (Traub et al. 1993), whereas NMDA currents are integrated over longer time periods because of their slow decay time constant (Bekkers and Stevens 1990; Salt 1986). Furthermore, shunting inhibition is expected to reduce the effects of excitatory currents on voltage.

In our granule cell model, low values of tonic inhibition were efficient in reducing the tail component of NMDA EPSPs, thus increasing the sensitivity on exact timing of synaptic inputs. This point is best illustrated by plotting the firing frequency of the granule cell as a function of the relative phase of two excitatory inputs activated at constant frequency. Figure 6, *A* and *B*, show plots of the normalized firing frequency (frequency at 0 phase set to 1) versus relative phase at various input frequencies, without and with a 0.1 nS inhibition, respectively. Inhibition introduces a timing dependence in integration of EPSPs that can be traced back to a suppression of NMDA tail potentials. Indeed, turning off inhibition and diminishing the NMDA component EPSPs by 15% produces a similar dependence on timing of EPSPs as in Fig. 6*B* (not illustrated).

The efficacy of two synaptic inputs depended on their phase relationship only for a limited range of input frequencies. With a value of 0.1 nS for the tonic inhibition, for instance, timing played an important role for the integration of synaptic inputs in a range of frequencies lying approximatively between 5 and 15 Hz (Fig. 6*B*). Increasing the value of tonic inhibition shifted toward higher values the range of input frequencies for which timing significantly influenced output firing frequency. This point is illustrated in Fig. 6*C*. For each value of tonic inhibition between 0.1 and 1.6 nS, we plotted on the vertical axis the interval of frequencies for which timing was significant. This interval (or "window") was defined as follows: the lower end of the interval is the lowest frequency for which "in phase" activity of two mossy fiber inputs was sufficient to trigger action potential firing, whereas "out of phase" activity of the same two inputs failed to reach threshold for action potential firing. The upper end of the window (upper horizontal bars in Fig. 6*C*) is the highest frequency at which stimulation of two mossy fibers in or out of phase still results in a difference in output firing of >25%. Plotting this

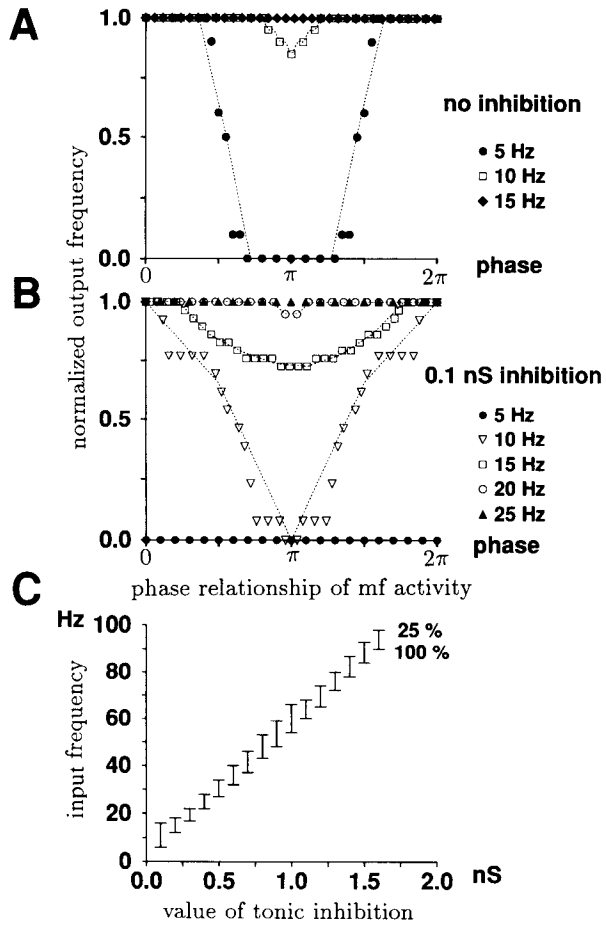

FIG. 6. Effects of tonic inhibition on the sensitivity to phase relationship of mossy fiber inputs. Two synapses were excited at constant frequency with different relative phases (0 phase is coincidental activation). *A*: without inhibition, the firing frequency depends on the relative phase of mossy fiber inputs only at 5 Hz stimulation frequency. *B*: with 0.1-nS inhibition the granule cell response depends on mossy fiber phase relationship at mossy fiber frequencies ≤15 Hz. *C*: range of mossy fiber input frequencies for which timing significantly affects the output frequency of the granule cell. The horizontal axis denotes different values of tonic inhibition. The vertical axis reports the range of mossy fiber frequencies for which stimulation in phase and out of phase result in output firing frequencies differing by >25%, lower end of the vertical bars denotes failure of "out phase" but not of "in phase" activity to trigger action potential firing.

timing window as a function of tonic inhibition (Fig. 6*C*) reveals that increasing inhibition shifts the timing window towards higher input frequency values. As will be emphasized in the DISCUSSION, this suggests that Golgi cell inhibition might adjust the sensitivity of granule cells on timing of mossy fiber inputs depending on the mean mossy fiber activity.

DYNAMICS OF EXCITABILITY. In our model, only two membrane conductances possess slow kinetics, the NMDA channel and the H channel. These conductances therefore might influence the integration, after an action potential, of subsequent excitatory inputs. We investigated this question by performing the following set of simulations: at time $t = 0$ ms, two mossy fiber synapses were activated whose compound EPSP triggered one action potential in the granule cell. Subsequent to this action potential, two further synapses (labeled *synapse 1* and *2*) were activated at different times, and the maximal time interval between these two synaptic events still able to trigger a second action potential was assessed. In Fig. 7, the time t_1 at which *synapse 1* was activated, measured from the deepest voltage reached by the AHP of the previous spike (upward arrow in the inset), is plotted on the horizontal axis. The vertical axis reports the maximal time Δt between the activation of *synapse 1* and *2* that still is able to trigger an action potential (i.e., *synapse 2* will trigger an action potential if and only if it is activated at a time t_2 smaller or equal to $t_1 + \Delta t$). The value of Δt immediately after the spike AHP is one-and-a-half times as high than at steady state. With increasing t_1, Δt diminishes and reaches a minimum (57 ms) at $t_1 = 200$ ms, when the NMDA potential triggering the first spike has vanished. After 200 ms, Δt slowly recovers to its steady-state value (62 ms), this is due to reactivation of the H current, which closed during the first spike (see Fig. 2*B3*).

The relative contribution of the NMDA and the H channels to the above effect are best isolated by examining the effects of modifying the NMDA or H channel conductances and time constants. The second plot of Fig. 7 illustrates the role of the NMDA current in the increased summation of EPSPs after a spike. At time $t_1 = 0$, that is, when the AHP of the first spike was deepest, we interrupted the simulation and set the NMDA current to 0 before resuming it. This has a dramatic effect on the summation of EPSPs: Δt almost drops to 0 immediately after the spike AHP and recovers as membrane potential increases toward its resting value and as the H channel reopens. In the same way, the time constant of the H channel influences the speed of recovery of Δt from its minimum value in Fig. 7 to steady state, whereas modifying the maximal conductance of the H channel changes the steady-state value of Δt (not illustrated). Inclusion of tonic inhibition shifted the filled curve of Fig. 7 along the vertical axis toward smaller values of Δt (~35 ms for 0.05 nS of tonic inhibition in each bulb) until

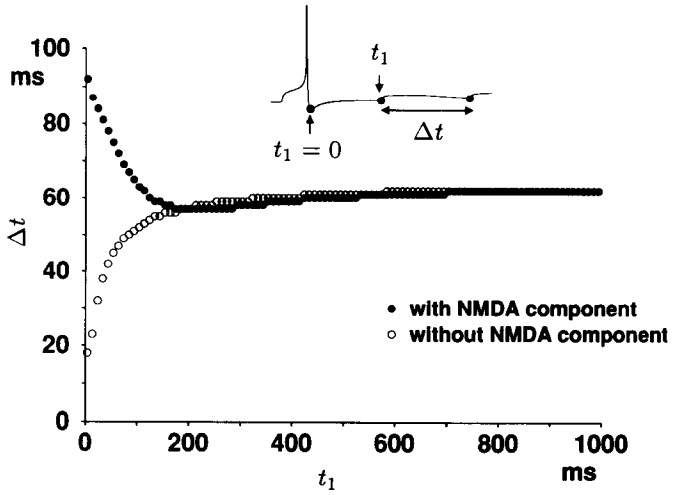

FIG. 7. Time window for synaptic integration: effect of NMDA tail currents after an action potential on the summation of subsequent synaptic inputs. The horizontal axis plots the time t_1 at which the first synapse is activated and the vertical axis the maximal time interval Δt between activation of *synapse 1* and *2* still able to elicit an action potential. *Inset*: the upward arrow denotes the 0 point of the t_1-axis and shows how Δt is measured.

tonic inhibition was strong enough to prevent the cell from firing under synchronous activation of two synaptic inputs.

DISCUSSION

Model

We have constructed a model of the turtle cerebellar granule cell to explore the synaptic integration of mossy fiber inputs in granule cells. The model is based on relatively detailed compartmental techniques but obviously its limitations have to be considered here. Because of the fact that experimental characterization of membrane currents of turtle granule cells under voltage-clamp conditions has not been performed yet, the model cannot be considered to be precise at the level of isolated membrane currents. We attempted to compensate for this by deriving, whenever possible, our kinetical models from available mammalian granule cells. Clearly this approach has its shortcomings: the electrophysiological data in mammalian granule cells was obtained from fairly young animals, and the microscopic behavior of channels in the two preparations is likely to be different. Nevertheless, mixing data from different species seems to be justifiable in view of the strong similarities between the membrane properties, at least on the phenomenological level, of turtles and mammalian cerebellar neurons, as has been extensively demonstrated in Purkinje cells (Hounsgaard and Midtgaard 1988; Llinás and Sugimori 1980). Furthermore we have performed extensive checks to verify that our results do not depend on the particular choice of our kinetic parameters.

Considering the responses of our model cell to intrasomatic current injections as compared with the corresponding responses seen in electrophysiologically recorded cells, it is plausible that the main membrane properties of turtle granule cells are well represented in our model. Small active currents might have been masked by larger currents under the experimental conditions employed to generate the data that we have used to constrain the parameter space of our model. However, the results and conclusions, which will be discussed below, do not depend on weakly expressed currents but rather on the following two main properties of granule cells:

1) The activation of synaptic conductances makes a negligible contribution to the overall membrane conductance during action potential firing. This results from the compactness of the cell, the small number of synapses, and the fact that during action potential firing, the membrane conductance is essentially generated by voltage-activated ion channels, which produce peak conductances 2 to 3 orders of magnitude larger than the synaptic conductances. This is constrained by the fact that granule cells have a morphology, which results in a compact spatial electrotonic structure and are able to fire fast and overshooting action potentials (Fig. 1*C*). In contrast, Bernander et al. (1991, Fig. 2*D*) have shown that for layer V pyramidal cells spontaneous synaptic activity can increase considerably the electrotonic distance of dendritic sites to the soma. However, in our model, tonic inhibition was able to modify significantly the input resistance of the cell and to compete with action potential generating mechanisms (Fig. 6). *2*) The activation of more than one mossy fiber is needed to fire granule cells. It has already been concluded from cat extracellular recordings in vivo that generally more than one synaptic input is needed to fire granule cells (Eccles et al. 1967), and recent intracellular recordings in rat and turtle cerebellar slices confirm this conclusion (E. D'Angelo, personal communication; Midtgaard, unpublished observations).

Thus the properties relevant for our conclusions are supported and consistent with experimental data.

Electrical compactness and spatial integration of EPSPs

Because of the very short electrotonic length of granule cell dendrites, synaptic potentials generated at the distal end of the dendrites spread almost unattenuated to the soma and other dendritic bulbs. We verified this by showing that the firing frequency of granule cells is essentially independent of the exact location of activated mossy fiber inputs (Fig. 4*A*). Furthermore we showed that dendritic synaptic current was equally efficient to drive the granule cell as direct intrasomatic current injection of the same size (Fig. 4*B*) and that attenuation of voltage transients is negligible due to the reduced cable structure of the granule cell. Considering only these points, the spatial integration of excitatory synaptic inputs in granule cells might be described by a model simpler than the one employed here (McCullogh and Pitts 1943). However, despite their spatial electrotonical compactness, these cells are not necessarily biochemically compact, and it might be possible that second messengers such as calcium are compartimentalized at each mossy fiber synapse in a way analogous to the one postulated for spines (see Koch and Zador 1993 and references given there). The present model also might serve as a basis for exploring these possibilities.

Temporal summation of EPSPs

Our simulations revealed that the NMDA component of suprathreshold mossy fiber EPSPs has an priming effect on subsequent mossy fiber inputs (Fig. 7). This might be of physiological significance under conditions where closely spaced mossy fiber inputs impinge on a single granule cell such as has been suggested for tactile sensory inputs, which consist of a short latency component and a longer-latency component mediated by a cerebro-cerebellar pathway (Gonzalez et al. 1993; Morissette et al. 1991). The simultaneous activation of two mossy fiber synapses as assumed in our simulations renders this facilitation effect maximal. However, even if most of the time mossy fiber synapses do not fire synchronously in vivo, this will not affect facilitation in a statistical sense (Gray et al. 1989). In addition to the slowly decaying NMDA receptor mediated current, also the H current influenced the temporal summation of EPSPs. In our simulations, the H current diminished the summation of subsequent synaptic inputs because it only slowly recovered from inactivation that occurred during action potentials. This effect was sensitive to the kinetics of the channel and to the number of channels open at rest. Because our model of the H current was not taken from recordings of turtle granule cells and in view of the diversity reported in the literature for the kinetics of inward rectification (Crepel and Penit-Soria 1986; Halliwell and Adams 1982; Mayer and Westbrook 1883; McCormick and Pape

1990), more precise conclusions on its role in mossy fiber integration will require an experimental characterization in granule cells. Notably, inward rectification also has been considered as a factor contributing to synaptic integration by other authors (Spain et al. 1987).

Effect of Golgi cell inhibition on synaptic integration

A large value of tonic inhibitory conductance was required to silence granule cells during simulations of high-frequency mossy fiber inputs. This is supported by the electrophysiological observation that spontaneous IPSPs were able to inhibit action potential firing (Fig. 1*C*, arrows) and is in line with extracellular recordings reported by Eccles and coworkers (1967) as well as with detailed morphological studies of glomeruli (Jakab and Hamori 1988). The possibility that Golgi cells might sample mossy fiber activity to adjust the firing threshold of granule cells was first considered by D. Marr (1969). In addition to this role of Golgi cell inhibition for "normalizing" mossy fiber to parallel fiber throughput with mossy fiber activity and for implementing a "sparse coding" of parallel fiber signals (see INTRODUCTION), the present simulations revealed an interesting new effect of feed forward and feed backward inhibition. The amount of Golgi cell inhibition also defines a window of frequencies in which the signal throughput in the mossy fiber parallel fiber system depends on the relative phase relationship between otherwise independent mossy fiber inputs (Fig. 6). If the synaptic weights of Golgi cell inhibition were adjusted such that this window follows changes in mean mossy fiber activity, granule cells would be tuned to preferentially transfer synchronized mossy fiber activity. This hypothesis requires experimental testing.

We thank M. Hines and R. Quadroni for providing us with versions of their simulators, E. D'Angelo and C. Staub for many helpful discussions, and K. Hepp for his attention and encouragement.

This project was supported by the Human Frontier Science Program.

Address for reprint requests: F. Gabbiani, Division of Biology, 139-74 California Institute of Technology, Pasadena, California 91125.

Received 5 November 1993; accepted in final form 20 April 1994.

REFERENCES

ARIEL, M. AND FAN, T. X. Electrophysiological evidence for a bisynaptic retinocerebellar pathway. *J. Neurophysiol.* 69: 1323–1330, 1993.

BEKKERS, J. M. AND STEVENS, C. F. Computational implications of NMDA receptor channels. *Cold Spring Harbor Symp. Quant. Biol.* 55: 131–135, 1990.

BERNANDER, Ö., DOUGLAS, R., MARTIN, K. A. C., AND KOCH, C. Synaptic background activity influences spatiotemporal integration in single pyramidal cells. *Proc. Natl. Acad. Sci. USA* 88: 11569–11573, 1991.

BLANTON, M. G., LO TURCO, J. J., AND KRIEGSTEIN, A. R. Whole cell recording from neurons in slices of reptilian and mammalian cerebral cortex. *J. Neurosci. Methods* 30: 203–210, 1989.

BORG-GRAHAM, L. J. *Modeling the somatic electrical response of hippocampal pyramidal neurons* (MS thesis). Cambridge, MA: The MIT Press, 1987.

BORG-GRAHAM, L. J. Modeling the non-linear conductances of excitable membranes. In: *Cellular Neurobiology: A Practical Approach,* edited by H. Wheal and J. Chad. New York: Oxford Univ. Press, 1991.

COLQUHOUN, D. AND HAWKES, A. G. On the stochastic properties of single ion channels. *Proc. R. Soc. Lond. B Biol. Sci.* 211: 205–305, 1981.

CONNOR, J. A. AND STEVENS, C. F. Prediction of repetitive firing behavior from voltage clamp data on isolated neurone soma. *J. Physiol. Lond.* 213: 31–53, 1971.

COOLEY, J. W. AND DODGE, W. A. Digital computer solutions for excitation and propagation of the nerve impulse. *Biophys. J.* 6: 583–599, 1966.

CREPEL, F. AND PENIT-SORIA, J. Inward rectification and low threshold calcium conductance in rat cerebellar Purkinje cells, an in vitro study. *J. Physiol. Lond.* 372: 1–23, 1986.

CULL-CANDY, S. G., MARSHALL, C. G., AND OGDEN, D. Voltage-activated membrane currents in rat cerebellar granule neurones. *J. Physiol. Lond.* 414: 179–199, 1989.

D'ANGELO, E., ROSSI, P., AND GARTHWAITE, J. Dual-component NMDA receptor currents at a single central synapse. *Nature Lond.* 346: 467–470, 1990.

D'ANGELO, E., ROSSI, P., PARATI, E., AND TAGLIETTI, V. Spontaneous to evoked NMDA currents in cerebellar granule cells. *Soc. Neurosci. Abstr.* 18: 565.14, 1992.

D'ANGELO, E., ROSSI, P., AND TAGLIETTI, V. Different proportions of *N*-methyl-D-aspartate and non-*N*-methyl-D-aspartate receptor currents at the mossy fibre-granule cell synapse of developing rat cerebellum. *Neuroscience* 53: 121–130, 1993.

D'ANGELO, E., ROSSI, P., AND TAGLIETTI, V. Voltage-dependent kinetics of *N*-Methyl-D-aspartate synaptic currents in rat cerebellar granule cells. *Eur. J. Neurosci.* 6: 640–645, 1994.

DEWAARD, M., FELTZ, A., AND BOSSU, J. L. Properties of a high-threshold voltage-activated calcium current in rat cerebellar granule cells. *Eur. J. Neurosci.* 3: 771–777, 1991.

ECCLES, J. C., ITO, M., AND SZENTÁGOTHAI, J. In: *The Cerebellum as a Neuronal Machine.* New York: Springer-Verlag, 1967.

EDGLEY, S. A. AND LIDIERTH, M. The discharges of cerebellar Golgi cells during locomotion in the cat. *J. Physiol. Lond.* 392: 315–332, 1987.

FAGNI, L., BOSSU, J. L., AND BOCKAERT, J. Activation of a large-conductance Ca-dependent K channel by stimulation of glutamate phosphoinositide-coupled receptors in cultured cerebellar granule cells. *Eur. J. Neurosci.* 3: 778–789, 1991.

FORTI, L. AND PIETROBON, D. Functional diversity of L-type calcium channels in rat cerebellar neurons. *Neuron* 10: 437–450, 1993.

GONZALEZ, L., SHUMWAY, C., MORISSETTE, J., AND BOWER, J. M. Developmental plasticity in cerebellar tactile maps: fractured maps retain a fractured organization. *J. Comp. Neurol.* 332: 487–498, 1993.

GRAY, C., KOENIG, P., ENGEL, A. K., AND SINGER, W. Oscillatory responses in cat visual cortex exhibit inter-columnar synchronization which reflects global stimulus properties. *Nature Lond.* 338: 334–337, 1989.

HALLIWELL, J. V. AND ADAMS, P. R. Voltage-clamp analysis of muscarinic excitation in hippocampal neurons. *Brain Res.* 250: 71–92, 1982.

HILLE, B. *Ionic Channels of Excitable Membranes.* Sunderland, MA: Sinauer Associates, 1992.

HINES, M. A program for simulation of nerve equations with branching geometries. *Int. J. Bio.-Med. Comput.* 24: 55–68, 1989.

HINES, M. The NEURON simulation program. In: *Neural Network Simulation Environments,* edited by J. Skrzypek. Norwell, MA: Kluwer Academic Publishers, 1993.

HODGKIN, A. L. AND HUXLEY, A. F. A quantitative description of membrane current and its application to conduction and excitation in nerve. *J. Physiol. Lond.* 117: 500–544, 1952.

HODGKIN, A. L. AND KEYNES, R. D. Movements of labelled calcium in squid giant axons. *J. Physiol. Lond.* 138: 253–281, 1957.

HOUNSGAARD, J. AND MIDTGAARD, J. Intrinsic determinants of firing pattern in Purkinje cells of the turtle cerebellum in vitro. *J. Physiol. Lond.* 402: 731–749, 1988.

HUGUENARD, J. R. AND MCCORMICK, D. A. Simulations of the currents involved in rhythmic oscillations in thalamic relay neurones. *J. Neurophysiol.* 68: 1373–1383, 1992.

JAHR, C. E. AND STEVENS, C. F. Voltage dependence of NMDA-activated macroscopic conductances predicted by single-channel kinetics. *J. Neurosci.* 10: 3178–3182, 1990a.

JAHR, C. E. AND STEVENS, C. F. A quantitative description of NMDA receptor-channel kinetic behavior. *J. Neurosci.* 10: 3178–3182, 1990b.

JAKAB, R. L. AND HAMORI, J. Quantitative morphology and synaptology of cerebellar glomeruli in the rat. *Anat. Embryol.* 179: 81–88, 1988.

KASE, M., MILLER, D. C., AND NODA, H. Discharge of Purkinje cells and mossy fibers in the cerebellar vermis of the monkey during saccadic eye movements and fixation. *J. Physiol. Lond.* 300: 539–555, 1980.

KIMURA, J., MIYAMAE, S., AND NOMA, A. Identification of sodium-calcium exchange current in single ventricular cells of guinea-pig. *J. Physiol. Lond.* 384: 199–222, 1987.

KOCH, C., POGGIO, T., AND TORRE, V. Retinal ganglion cells: a functional

interpretation of dendritic morphology. *Proc. R. Soc. Lond. B Biol. Sci.* 298: 227–264, 1982.

KOCH, C. AND ZADOR, A. The function of dendritic spines: devices subserving biochemical rather than electrical compartimentalization. *J. Neurosci.* 13: 413–422, 1993.

KRIEGSTEIN, A. R. AND CONNORS, B. W. Cellular physiology of the turtle visual cortex: Synaptic properties and intrinsic circuitry. *J. Neurosci.* 6: 178–191, 1986.

LLINÁS, R. AND SUGIMORI, M. Electrophysiological properties of in vitro Purkinje cell somata in mammalian cerebellar slices. *J. Physiol. Lond.* 305: 171–195, 1980.

MARCHETTI, C., CARAGNANI, C., AND ROBELLO, M. Voltage-dependent calcium currents in dissociated granule cells from the rat cerebellum. *Neuroscience* 43: 121–133, 1991.

MARR, D. A theory of cerebellar cortex. *J. Physiol. Lond.* 202: 437–470, 1969.

MASCAGNI, M. V. Numerical methods for neuronal modeling. In: *Methods in Neuronal Modeling*, edited by C. Koch and I. Segev. Cambridge, MA: The MIT Press, 1989.

MAYER, M. L. AND WESTBROOK, G. L. A voltage-clamp analysis of inward (anomalous) rectification in mouse spinal sensory ganglion neurones. *J. Physiol. Lond.* 340: 19–45, 1983.

MCCORMICK, D. A. AND PAPE, H.-C. Properties of a hyperpolarization-activated cation current and its role in rhythmic oscillation in thalamic relay neurons. *J. Physiol. Lond.* 431: 291–318, 1990.

MCCULLOGH, W. S. AND PITTS, W. A logical calculus of the ideas immanent in nervous activity. *Bull. Math. Biophys.* 5: 115–133, 1943.

MEL, B. W. NMDA-based pattern discrimination in a modeled cortical neuron. *Neural Comput.* 4: 502–517, 1992.

MEL, B. W. Synaptic integration in an excitable dendritic tree. *J. Neurophysiol.* 70: 1086–1101, 1993.

MIDTGAARD, J. Membrane properties and synaptic responses of Golgi cells and stellate cells in the turtle cerebellum in vitro. *J. Physiol. Lond.* 457: 329–354, 1992.

MOCZYDLOWSKI, E. AND LATORRE, R. Gating kinetics of Ca-activated K-channels from rat muscle incorporated into planar lipid bilayers. *J. Gen. Physiol.* 82: 511–542, 1983.

MORISSETTE, J., LEE, M., AND BOWER, J. M. Temporal relationship between cerebral cortical and cerebellar responses to tactile stimulation in the rat. *Soc. Neurosci. Abstr.* 17: 552.6, 1991.

MUGNAINI, E., ATLURI, R. L., AND HOUK, J. C. Fine structure of granular layer in turtle cerebellum with emphasis on large glomeruli. *J. Neurophysiol.* 37: 1–29, 1974.

MULLINS, L. J. A mechanism for Na/Ca transport. *J. Gen. Physiol.* 70: 681–695, 1977.

NAPPER, R. M. A. AND HARVEY, R. J. Quantitative study of the Purkinje cell dendritic spines in the rat cerebellum. *J. Comp. Neurol.* 274: 168–177, 1988a.

NAPPER, R. M. A. AND HARVEY, R. J. Number of parallel fibers synapses on an individual Purkinje cell in the cerebellum of the rat. *J. Comp. Neurol.* 274: 168–177, 1988b.

NEHER, E. AND AUGUSTINE, G. J. Calcium gradients and buffers in bovine chromaffin cells. *J. Physiol. Lond.* 450: 273–301, 1992.

QUADRONI, R. *Realistic models of the medial vestibular nuclei neurons* (PhD thesis). Zurich, Switzerland: ETH, 1993.

RALL, W. Theoretical significance of dendritic trees for neuronal input-output relations. In: *Neural Theory and Modeling*, edited by R. F. Reiss. Standford, CA: Standford Univ. Press, 1964.

ROBINSON, R. A. AND STOKES, R. H. *Electrolyte solutions.* London: Butterworths, 1955.

SAH, P., GIBB, A. J., AND GAGE, P. W. Potassium current activated by depolarization of dissociated neurons from adult guinea pig hippocampus. *J. Gen. Physiol.* 92: 263–278, 1988.

SALA, F. AND HERNANDEZ-CRUZ, A. Calcium diffusion modeling in a spherical neuron. *Biophys. J.* 57: 313–324, 1990.

SALT, T. E. Mediation of thalamic sensory input by both NMDA and non-NMDA receptors. *Nature Lond.* 322: 263–265, 1986.

SILVER, R. A., TRAYNELIS, S. F., AND CULL-CANDY, S. G. Rapid-time-course miniature and evoked excitatory currents at cerebellar synapses in situ. *Nature Lond.* 355: 163–166, 1992.

SLESINGER, P. A. AND LANSMAN, J. B. Inactivation of calcium currents in granule cells cultured from mouse cerebellum. *J. Physiol. Lond.* 435: 101–121, 1991.

SOFTKY, W. R. AND KOCH, C. The highly irregular firing of cortical cells is inconsistent with temporal integration of random EPSPs. *J. Neurosci.* 13: 334–350, 1993.

SPAIN, W. J., SCHWINDT, P. C., AND CRILL, W. E. Anomalous rectification in neurons from cat sensorimotor cortex in vitro. *J. Neurophysiol.* 57: 1555–1575, 1987.

TRAUB, R. D., MILES, R., AND JEFFERYS, J. G. R. Synaptic and intrinsic conductances shape picrotoxin-induced synchronized after discharges in the guinea-pig hippocampal slice. *J. Physiol. Lond.* 461: 525–547, 1993.

TRAUB, R. D., WONG, R. K. S., MILES, R., AND MICHELSON, H. A model of a CA3 hippocampal pyramidal neuron incorporating voltage-clamp data on intrinsic conductances. *J. Neurophysiol.* 66: 635–650, 1991.

VAN KAN, P. L., GIBSON, A. R., AND HOUK, J. C. Movement-related inputs to intermediate cerebellum of monkeys. *J. Neurophysiol.* 69: 74–94, 1993.

VU, E. T. AND KRASNE, F. B. Evidence for a computational distinction between proximal and distal neuronal inhibition. *Science Wash. DC* 255: 1710–1712, 1992.

YAMADA, W. M., KOCH, C., AND ADAMS, P. R. Multiple channels and calcium dynamics. In: *Methods in Neuronal Modeling*, edited by C. Koch and I. Segev. Cambridge, MA: The MIT Press, 1989.

CORRIGENDA

Volume 72, August 1994

Pages 999–1000: F. Gabbiani, J. Midtgaard, and T. Knöpfel, "Synaptic Integration in of Cerebellar Granule Cells." Table 1 contains the following two mistakes.

1) The backward rate function for the activation of the high-voltage activated conductance should read

$$-0.02(V + 8.9)/\{1 - e^{[0.2(V+8.9)]}\}$$

instead of

$$-0.02(V - 8.9)/[1 - e^{-0.2(V-8.9)}].$$

2) The forward rate function for the inactivation of the delayed rectifier potassium tance should read

$$0.0007 + 6 \cdot 10^{-5} e^{[-0.08(V+46)]}$$

instead of

$$0.0007 + 6.5e^{[-0.08(V+46)]}.$$

The authors thank Dr. H. Lu for bringing these two mistakes to their attention.